Revisiting the Atomistic Structures at the Interface of Au(111) Electrode–Sulfuric Acid Solution

Yuan Fang, Song-Yuan Ding, Meng Zhang, Stephan N. Steinmann, Ren Hu, Bing-Wei Mao, Juan M Feliu, Zhong-Qun Tian

Revisiting the atomistic structures at the interface of Au(111) electrode-sulfuric acid solution

Yuan Fang,[†] Song-Yuan Ding,[†,*] Meng Zhang,[†,|] Stephan N. Steinmann,[‡] Ren Hu,[†] Bing-Wei Mao,[†,*] Juan M. Feliu,[§,*] and Zhong-Qun Tian[†]

[†]State Key Laboratory of Physical Chemistry of Solid Surfaces (PCOSS), Collaborative Innovation Center of Chemistry for Energy Materials (iChEM), and Department of Chemistry, College of Chemistry and Chemical Engineering, Xiamen University, Xiamen 361005, China.

[‡]Université de Lyon, Ecole Normale Supérieure de Lyon, CNRS, Université Lyon 1, Laboratoire de Chimie UMR 5182, 46 Allée d'Italie, F-69364 Lyon, France.

[§]Instituto Universitario de Electroquímica, Universidad de Alicante, Carretera San Vicente del Raspeig s/n, E-03690 San Vicente del Raspeig, Alicante, Spain.

[|]Meng Zhang's present address is BTR New Material Group CO., LTD., GuangMing New District, Shenzhen 518106, China.

Supporting Information Placeholder

ABSTRACT: Knowledge of atomistic structures at solid/liquid interfaces is essential to elucidate interfacial processes in chemistry, physics, and materials sciences. The ($\sqrt{3}\times\sqrt{7}$) structure associated with a pair of sharp reversible current spikes in the cyclic voltammogram on a Au(111) electrode in sulfuric acid solution, represents one of the most classical structures at electrode/electrolyte interfaces. Although more than ten adsorption configurations have been proposed by more than ten groups in the past four decades, the atomistic structure remains ambiguous and is consequently an open problem in electrochemistry and surface science. Herein, by combining high-resolution electrochemical scanning tuning microscopy, electrochemical infrared and Raman spectroscopies, and in particular, the newly developed quantitative computational method for electrochemical infrared and Raman spectra, we unambiguously reveal that the adstructure is Au(111)($\sqrt{3}\times\sqrt{7}$)-($SO_4\cdots w_2$) with a sulfate anion (SO_4*) and two structured-water molecules (w_2*) in a unit cell, and the crisscrossed $[w\cdots SO_4\cdots w]_n$ and $[w\cdots w\cdots]_n$ hydrogen-bonding network comprises the symmetric adstructure. We further elucidate that the electrostatic potential energy dictates the proton affinity of sulfate anions, leading to the potential-tuned structural transformations. Our work enlightens the structural details of the inner Helmholtz plane and thus advances our fundamental understanding of the processes at electrochemical interfaces.

INTRODUCTION

Solid/liquid interfacial structures play crucial roles in determining chemical processes, such as electrochemistry, catalysis, corrosion, composite formation, wear and wetting.[1-3] At electrode/electrolyte solution interfaces, specifically adsorbed anions e.g., sulfate, superoxide, and halide anions and water solvent molecules can reconstruct the interfacial structures, and thus affect the thermodynamics and kinetics of electrode processes.[4-6] It is of fundamental importance to probe the atomistic details of the electrochemical (EC) interfaces.

Sulfate or bisulfate anions adsorbed on the surface of an atomically flat Au(111) electrode in sulfuric acid is one of the most classical adsorption systems in the long history of interfacial electrochemistry and surface science.[7-8] In 1984, Scherson *et al.* first observed a pair of sharp reversible current spikes at ~1.06 V *vs*. SHE below the oxygen evolution potential in the cyclic voltammogram (CV) of Au(111) single-crystal electrodes in H_2SO_4 aqueous solutions, and attributed the spikes to a phase transition of the anion adlayer.[9] Since then a series of *in-situ* electrochemical scanning tunneling microscopy (EC-STM) and electrochemical infrared (EC-IR) spectroscopy have been employed by more than ten distinguished groups in the field of interfacial electrochemistry and surface science to elucidate the detailed structure and process associated with the current spikes. In 1992, Magnussen *et al.* employed EC-STM to firstly observe a ($\sqrt{3}\times\sqrt{7}$) patterned adstructure near the sharp current spikes and proposed it to be composed of adsorbed bisulfate anions (HSO_4*, the charge of the electro-adsorbed species is usually fractional and depends on the applied potential; * denotes the adsorbed species).[10] In 1994, the Weaver group assigned the possible adstructure as the sulfate anion co-adsorbed with a hydronium cation $SO_4\cdots H_3O$* by performing the combined

EC-STM and EC-IR method.[11] The Osawa group interpreted the measured synchronous 2D EC-IR spectra on the ultra-flat Au film electrode as a sulfate anion co-adsorbed with one water molecule (w) as $SO_4\cdots w^*$ with two possible hydrogen-bonding configurations.[12] Several possible configurations have been proposed according to the empirical assignments of the bands observed in the EC-IR spectra and/or qualitative assignments of the fuzzy features in the EC-STM images.[13-15] In addition, the Lipkowski and Wieckowski groups deduced SO_4^* instead of HSO_4^* by chronocoulometry and radiochemistry.[16] Theoretically, the Jacob group concluded that the configuration with $SO_4\cdots H_3O^*$ is the most stable configurations by density functional theory (DFT) based binding energies of eight possible configurations.[17] However, they did not consider the applied potential and neglected solvation effects. In short, most groups supported that the main adsorbates are sulfate anions.

Although more than ten adsorption configurations for the $Au(111)/H_2SO_4$ system have been proposed in the past four decades, the atomistic structure of the Au(111)(√3×√7)-adsorbate associated with the current spikes at approximately 1.06 V remains ambiguous. Consequently, it is one of the open problems in electrochemistry and surface science with several unsolved issues: (1) Are are water or hydronium molecules co-adsorbed with each sulfate or bisulfate? And if so, how many? (2) What are the detailed hydrogen-bonding networks that comprise the two-dimensional crystalline adstructure? Importantly, such observations and open questions also exist for other $M(111)/H_2SO_4$ solution interfaces (M = Pt, Rh, Cu, Ir, and Pd),[18-22] where the (√3×√7) adstructures prevail as revealed by EC-STM, but the atomistic structures of these interfaces are also ambiguous.[13,23-25]

The difficulties in unambiguously determining the adstructure of the Au(111)(√3×√7)-adsorbate in previous studies are threefold: (1) The spatial resolution of the EC-STM twenty years ago is not sufficiently high to resolve the atomistic details of adsorbates as sulfate or bisulfate anions, water molecule or hydronium cation; (2) The vibrational frequencies of the EC-IR spectra reported in the literature are higher than 900 cm^{-1} feature only one or two vibrational modes associated with the sulfate or bisulfate species, while vibrational modes with frequencies below 500 cm^{-1}, associated with the adsorbate-surface interactions, are missing; (3) There are no quantitative theoretical methods to calculate the EC-IR and EC-Raman spectra from single crystal electrode/electrolyte interfaces, which play essential roles in precisely interpreting the measured spectra. Therefore, we herein combine the latest experimental and corresponding computational methods to unambiguously reveal the atomistic arrangements of adsorbed anions in association with co-adsorbed species, and to comprehensively understand the interactions in the inner Helmholtz plane, which is the heart of the electric double layer at the interface.[1,26-29]

In this study, we employed high-resolution EC-STM combined with DFT calculation to quantitatively assign the atomistic arrangement of the adstructure. The EC-IR spectral data in the literature, combined with our *in-situ* electrochemical shell-isolated nanoparticle-enhanced Raman spectroscopy (EC-SHINERS) with 4–6 orders of magnitude enhancement in Raman signals of adsorbates on metallic (e.g., Au, Cu, Pt, Rh) single-crystal electrodes,[30-33] were employed to unveil the chemical bonding of both sulfate anions and water molecules in the (√3×√7) adstructure. To accurately interpret the features of the experimental spectra, we employed our newly developed computational method to calculate the EC-IR and EC-Raman spectra of nine possible configurations of Au(111)(√3×√7)-X (X denotes the speculated adsorbates).[34] This computational method quantitatively calculates the vibrational frequencies and, importantly, the spectral intensities of adstructures at the single-crystal electrodes/liquid interfaces by simultaneously considering the surface charge and solvation effect. We found that the calculated EC-STM image, EC-IR and EC-Raman spectra of the Au(111)(√3×√7)-($SO_4\cdots w_2$) configuration perfectly match the respective experimental observations. Finally, we sketched a reaction free energy (ΔG_{re}) diagram[25] by calculating the potential-dependent Gibbs free energies $G_{ads}(V)$ of all configurations to further confirm the energetic preference for the adstructure, Au(111)(√3×√7)-($SO_4\cdots w_2$). The diagram also reveals that the potential-dependent interplay between the proton affinity of sulfate anions and the electrostatic potential energy determines the structural transformation at the EC interfaces. Our work not only elucidates the detailed adsorption configuration at the $Au(111)/H_2SO_4$ solution interface, but also provides a paradigm for the combined theory/experimental tool kit to unveil the atomistic structures at electrodes/electrolyte interfaces.

EXPERIMENTAL SECTION

Chemicals. Sulfuric acid (96%) was purchased from Merck. Deionized Milli-Q water (resistivity of 18.2 MΩ cm) was used for all aqueous solutions.

Preparation of the Au(111) single crystal electrodes. The Au(111) half-bead single crystal electrodes were prepared following Clavilier's method[35] and used as the working electrodes. The surface area of the Au(111) electrode is 3.733 mm^2.

Electrochemical measurements. Cyclic voltammetry (CV) experiments were performed on a CHI electrochemical workstation (CHI 660D, CH Instrument). A Pt wire was used as the counter electrode and a reversible hydrogen electrode (RHE) connected to the cell via a Luggin capillary was used as the reference electrode.

STM measurements. *In-situ* STM measurements were performed on a Nanoscope V STM instrument (Veeco, Santa Barbara, CA). Mechanically cut Pt/Ir tips were used, which were insulated by apiezon wax or thermosetting glue to reduce the electrochemical current. The STM works in the constant current mode, and the scanning range is 4 nm × 4 nm.

Raman spectroscopic measurements. Pinhole-free Au@SiO2 nanoparticles with a Au core diameter of ~55 nm and a SiO_2 shell thickness of ~3 nm were synthesized according to Li's methods.[30] $Au@SiO_2$ NPs were introduced onto the Au(111) single crystal electrodes by dropping a dilute $Au@SiO_2$ sol solution, followed by the evaporation of the

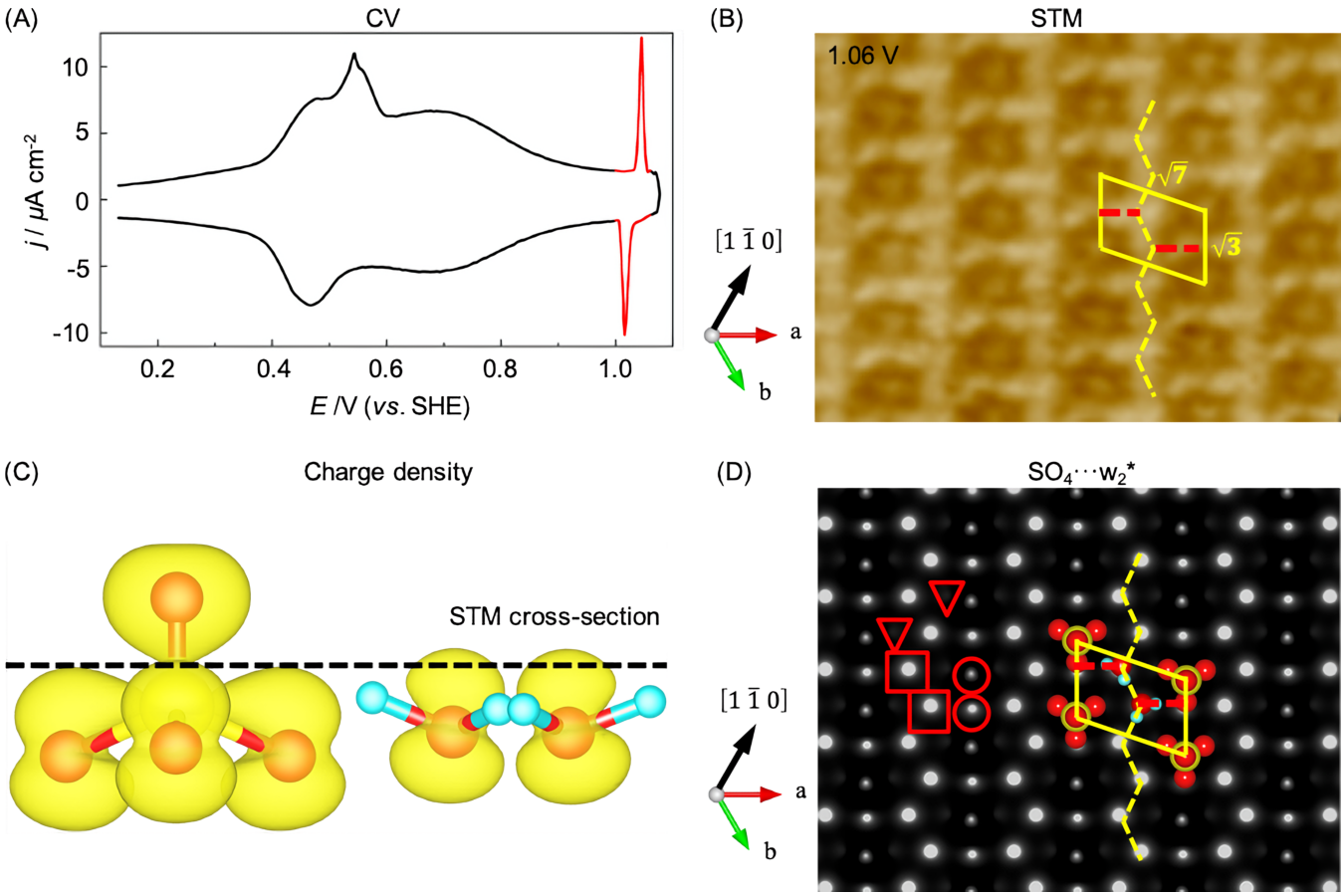

Figure 1. Probing atomistic structures in the Au(111)/H_2SO_4 solution interface. (A) Cyclic voltammetry curve of Au(111) in 0.1 M H_2SO_4 aqueous solution, scan rate: 20 mV/s. (B) High resolution STM image at 1.06 V *vs*. SHE. (C) Distribution of charge density of the SO_4···w_2* configuration near the Fermi level E_F. The unit vectors ***a***, ***b*** are the basic vectors of the Au(111)(1×1) along with the **[1 0 $\bar{1}$]** and **[0 1 $\bar{1}$]** directions, respectively. (D) Calculated STM image of the Au(111)(√3×√7)-(SO_4···w_2) configuration. The basic vectors of Au(111)(√3×√7) are defined as 2***b*** – ***a*** (√3 direction) and 2***a*** + ***b*** (√7 direction), respectively. The main maxima, secondary maxima and minima spots correspond to red panes, circle and triangle frames, respectively.

solvent water in the sol. Raman spectra were acquired with a Renishaw InVia Qontor confocal Raman instrument. The excitation line was 632.8 nm from He-Ne laser. Electrochemical control was maintained using the CHI electrochemical workstation. A homemade spectro-electrochemical cell with a Pt wire counter electrode and RHE reference electrode was used for the EC-SHINERS experiments.

Density functional theory calculations. The metal surfaces were modeled as a symmetric Au(111)(√3×√7) slab with a lattice constant of 4.21 Å and a thickness of 7 layers in a periodic box of 78.03 Å (the middle three layers were frozen in the bulk position). The first-principles computations were performed using the Vienna ab initio simulation package (VASP) with projector augmented wave (PAW) pseudopotentials.[36-37] The alternative revision of the Perdew-Burke-Ernzerhof functional, RPBE, was employed to calculate the chemisorption energies of the adsorbates on the Au(111) surface.[38] We considered a 550 eV plane-wave energy cut-off and integrated the Brillouin zone with a 5×5×1 Γ-centered K-point mesh for a (√3×√7) unit cell. The self-consistent field procedure was repeated until a precision of 1×10^{-9} eV in the total energy. All geometries were optimized to reach residual forces on all atoms lower than 0.01 eV/Å. The simulated STM images are constructed on the basis of Tersoff-Hamann theory with a bias voltage of + 0.85 V and were visualized using the p4vasp program.[39] To calculate the EC-IR and -Raman spectra, VASPsol implementation was employed to mimic surface solvation effect.[40] The relative permittivity ε_r and ionic strength I were set to 78 and 0.3 M (corresponding to Debye screening length λ, 5.5 Å), respectively. The surface tension was set to zero (no cavitation energy). Finite difference method was employed to calculate the IR and Raman spectra. The differential step size of Cartesian coordinates Δx and electrostatic field strengths along the z axis ΔG_z were set to 0.01 Å and 0.1 V/Å, respectively. The detailed computational methods of EC-IR and -Raman spectra were listed in ref. 34. Other computational details are provided in the SI.

RESULTS AND DISCUSSION

A typical CV of the Au(111) electrode in 0.1 M H_2SO_4 was recorded from 0.05 to 1.2 V *vs*. SHE away from the characteristic voltages regarding hydrogen or oxygen evolution processes (Figure 1A). The CV shows a pair of sharp spikes at approximately 1.06 V (red lines), which is consistent with the results from the literature,[15,41-42] and indicates the high quality of the Au(111) single-crystal electrode in this work.

Determining the adstructure from nine possible configurations at high potentials. In Figure 1B, the measured EC-STM image at potentials of 1.06 V and above

(1.06–1.20 V, high potentials) exhibits the well-known (√3×√7) adstructure rotated by 19.1° from the [1 $\bar{1}$ 0] direction of the Au(111) surface, with the bright spots at the corners of the yellow (√3×√7) frame. The STM image shows many detailed features that were not resolved before.[10-11,15,42] In particular, we observed zig-zag chains (dashed yellow line segments along the √3 direction) and two lobes (dashed red lines along the direction of ***a***) going through and inside the yellow frame, respectively.

To unveil the observed ultrafine features in the measured STM image, we first constructed thirteen possible Au(111)(√3×√7)-X configurations, which yielded nine unique structures after geometry optimization (Figure 2). They span suggested configurations from the literature[10-13,15,17,23,43-44] and our initial guesses. We then compared the various simulated EC-STM images with the measured one. See detailed atomistic labels in Figure 2A and the caption of Figure 2.

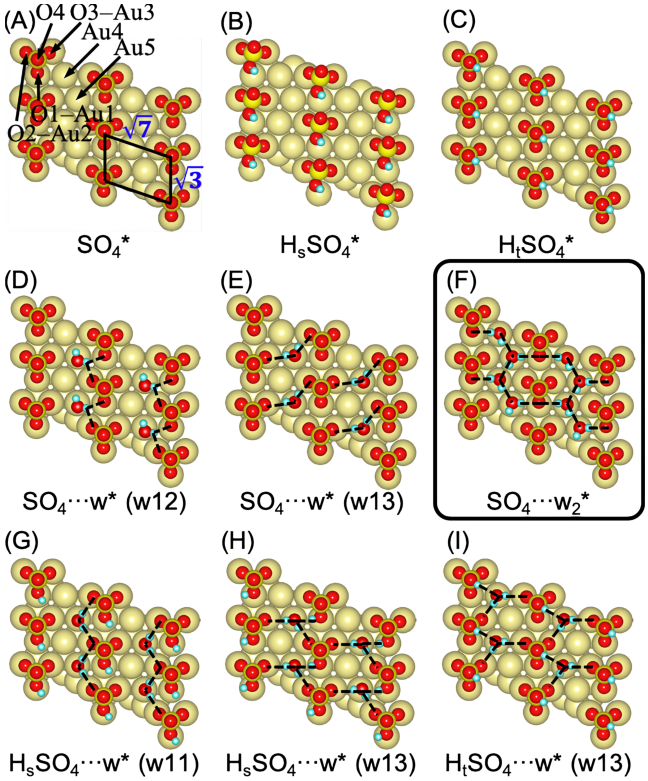

Figure 2. Nine proposed and optimized Au(111)(√3×√7)-X configurations. (A) SO_4*; (B) and (C) H_sSO_4* and H_tSO_4* with H bonding with O2 and O4, respectively; (D) and (E) SO_4···w* (w12) and SO_4···w* (w13) consist of a sulfate anion and a co-adsorbed water molecule with SO_4···w* hydrogen-bonds through O1 and O2 or O1 and O3, respectively; (F) SO_4···w_2* consists of a sulfate anion and a co-adsorbed dual-water (w_2) molecules; (G) and (H) H_sSO_4···w* (w11) and H_sSO_4···w* (w13) consist of a bisulfate anion with H bonding with O2 and a co-adsorbed water molecule with H_sSO_4···w* hydrogen-bonds through O1 and O1 or O1 and O3 from different H_sSO_4* molecules; (I) H_tSO_4···w*(w13) consists of a bisulfate anion with H bonding with O4 and a co-adsorbed water molecule with H_tSO_4···w* hydrogen-bonds through O1 and O3 from different H_tSO4* molecules. The golden, yellow, red, and cyan balls denote Au, S, O, and H atoms, respectively.

More convincingly than the calculated STM patterns of other configurations (Figure S1), the calculated STM pattern (Figure 1C) of Au(111)(√3×√7)-(SO_4···w_2) perfectly matches the measured one at high potentials (Figure 1B). The bright and isolated spots are assigned to the upmost oxygen atoms (denoted as O4 in Figures 2A and 2F) of SO_4*; the zig-zag chains are assigned to hydrogen-bonded dual-water molecules. The two lobes are assigned to the side oxygen atoms (denote as O2 atoms in Figure 2A and 2F) of two adjacent SO_4* molecules (along the √7 direction) which are hydrogen-bonded with the two water molecules. As we know, the spot brightness depends on the STM cross-section of the oxygen charge density near the Fermi level E_F in Au(111)(√3×√7)-X. In Figure 1C, the main maxima spots (marked with two red open squares, aligned along the zig-zag chains), secondary maxima spots (marked with two red open circles, aligned along the √3 direction), and minima spots (marked with two red open triangles, intertwined with the main maxima spots) in the (√3×√7) unit cell, are associated with the charge densities of O atoms from the dual-water molecules hydrogen-bonded with each other, O2 and O4 atoms of the SO_4*, and O1 and O3 atoms of the SO_4*, respectively, since their cross-sections decrease in turn (Figure 1D). The simulated STM images of other configurations failed to reproduce either the zig-zag feature or the two-lope feature. Our finding identifies the experimentally observed structure as highly symmetric crisscrossed [w···SO_4···w] and [w···w···]$_n$ hydrogen-bonding network of the adstructure Au(111)(√3×√7)-(SO_4···w_2).

EC-IR spectroscopy can provide information on the sulfate anions, and particularly reveals rich vibrational information concerning the co-adsorbed water molecule or hydronium cation and in the adstructure of Au(111)(√3×√7)-X at the high potentials. The EC-IR spectrum (the dark red curve in Figure 3A) at 1.06 V measured by Ataka *et al.*,[12] features three main bands at 955, 1183, and 1650 cm^{-1}, which have been assigned to the symmetric SO_4 stretching mode $\nu_s(SO_4)$, S–O bond stretching mode ν(SO) of SO_4*, and bending mode of w*, $\delta(H_2O)$ by the authors. The experimental assignment alone can only provide an ambiguous determination of adstructures. However, the simulated EC-IR spectra of all possible configurations, accompanied with the measured EC-IR spectra evidentially help us to exclude most of the candidate configurations. Figures 3A and 3B show that the possible configurations with H_tSO_4···w* (w13), H_sSO_4···w* (w13), or H_sSO_4···w* (w11) can be excluded since the calculated bands at 1226 or 1243 cm^{-1} assigned to the ν(SO) mode of HSO_4*, cannot be observed in the measured EC-IR spectrum. The possible configurations with SO_4···w* (w12), SO_4*, or H_sSO_4*, H_tSO_4* can also be excluded due to the absence of the $\delta(H_2O)$ bands at around 1650 cm^{-1}. Additionally, the SO_4···w* (w13) configuration can be excluded because a pair of splitting bands at 944 and 974 cm^{-1} due to the decrease of the sulfate anion symmetry, poorly match the single band at 956 cm^{-1} in the measured EC-IR spectrum. The previously suggested well-known Au(111)(√3×√7)-(SO_4···H_3O) configuration[17,44] can be excluded for two reasons: (i) The characteristic hydronium band at around 1700 cm^{-1} cannot be observed in the EC-IR spectra at high potentials;[45] (ii) Computationally, configurations with a co-adsorbed hydronium cannot be optimized at high potentials, but converge to HSO_4···w* configurations. In summary, only the calculated EC-IR

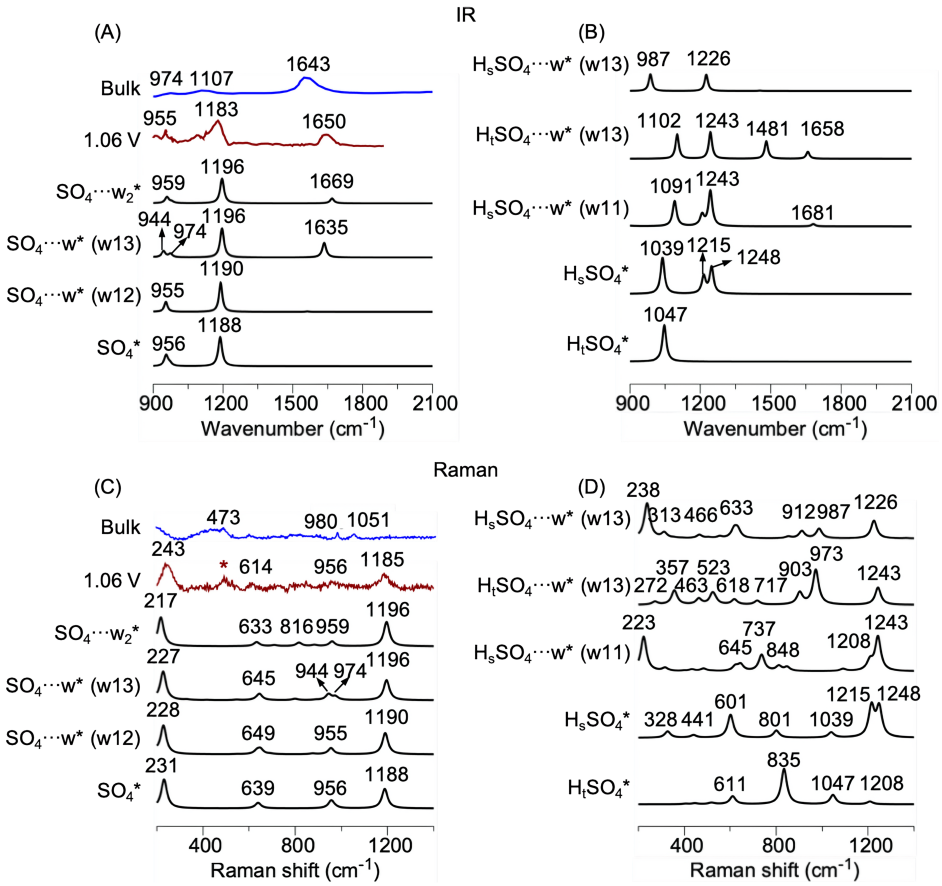

Figure 3. Calculated EC-IR and -Raman spectra of the Au(111)(√3×√7)-X configurations at 1.06 V *vs*. SHE. EC-IR spectra of the configurations containing sulfate anions in (A) or bisulfate anions in (B). EC-Raman spectra of the configurations containing sulfate anions in (C) or bisulfate anions in (D). The blue curves in panel A and C, respectively, denote the measured IR and Raman spectrum of bulk solution. The dark red curves in panel A and C, respectively, denote the measured EC-IR and -Raman spectrum at 1.06 V. The measured IR spectra were adapted from ref. 12 with permission, copyright (1998) American Chemical Society.

spectrum of Au(111)(√3×√7)-(SO_4···w_2) matches well the measured one.

To understand the IR activity of the $\delta(H_2O)$ bands of the possible configurations, we analyzed the orientation of the dipole of w*, θ_w, defined as the included angle between the dipole moment of w* and the surface normal of Au(111). The θ_w angels in SO_4···w* (w12) and H_sSO_4···w* (w13) are 79° and 98°, respectively. As a result, the $\delta(H_2O)$ bands of the two possible configurations are almost IR-inactive according to the surface selection rule of surface IR spectroscopy on metal surfaces.[26] In SO_4···w_2*, the θ_w angles of both water molecules are almost identical (67°). The band centered at 1669 cm^{-1} of SO_4···w_2* is assigned to the symmetric bending mode $\delta_s(H_2O)$ of dual hydrogen-bonded water molecules, and is IR-active; the anti-symmetric bending mode $\delta_{anti}(H_2O)$ centered at 1685 cm^{-1} is, however, IR-inactive.

The EC-Raman spectroscopy has the advantage over the EC-IR counterpart to provide much richer vibrational fingerprint information on the sulfate or bisulfate anions with vibrational frequencies of 100–1300 cm^{-1}. However, it is difficult to obtain high signal-to-noise EC-SHINERS spectra in this study due to the weak Raman activity of the interfacial species in this system. The primarily measured potential-dependent Raman spectra are shown in Figure S2. For comparison with the measured EC-Raman spectra, the Raman spectrum from the bulk solution was taken first (the blue curve in Figure 3C). Three main bands centered at 473, 980, and 1051 cm^{-1} are shown and assigned to the combinational SO_2 wagging and rocking modes $\rho_{w+r}(SO_2)$, symmetric SO_4 stretching mode $\nu_s(SO_4)$, and symmetric SO_3 stretching mode $\nu_s(SO_3)$, respectively (See the detailed analyses in SI 5 and modes in Figures S3–S5). The EC-SHINER spectrum at 1.06 V (dark red curve in Figure 3C) and above shows four bands at 243, 614, 956, and 1185 cm^{-1}. The considerable difference between the EC-SHINER spectrum and the bulk Raman spectrum indicates that the four bands arise from vibrational modes of the interfacial species instead of bulk species.

The calculated EC-Raman spectra for the configurations that containing adsorbed sulfate anions (SO_4···w_2*, SO_4···w* (w12), and SO_4* (Figure 3C)) show four bands at 217–231, 633–649, 944–959 and 1188–1196 cm^{-1}, which in some extent agree with the measured spectrum counterparts at 1.06 V. The SO_4···w* (w13) configuration can, however, be excluded, as the pair of splitting bands at 955 cm^{-1} cannot be observed in the measured one. Moreover, the Stark tuning slopes (STS, defined as the slope of the vibrational frequency as a function of the applied potential) of the four bands in the measured Raman spectra also in some extent agree with the calculated Raman spectra of the three configurations counterparts, as shown in Table 1. Particularly, the 956 and 1185 cm^{-1} frequencies of the measured EC-Raman bands at 1.06 V perfectly match the frequencies 955 and 1183 cm^{-1} of the measured EC-IR spectrum at 1.06 V (Figure 3A and 3C, dark red curves). Furthermore, the STS of the 1185 cm^{-1} band (59 $cm^{-1}V^{-1}$) in the measured EC-Raman spectra perfectly

matches those of the measured EC-IR band at 1189 cm^{-1} (45 $cm^{-1}V^{-1}$) by Edens *et al.*[11] and the IR band at 1183 cm^{-1} (60 $cm^{-1}V^{-1}$) by Ataka *et al.*[12] Therefore, the observed bands at 243, 614, 956, and 1185 cm^{-1} of the Raman spectrum at 1.06 V, are assigned to the out-of-surface translational-like mode of SO_4* T(Au–SO_4), symmetric SO_3 bending mode $\delta_s(SO_3)$, $\nu_s(SO_4)$ mode, and ν(SO) mode (Figure S6–S9), respectively.

Table 1. STSs ($cm^{-1}V^{-1}$) of the vibrational frequencies for the adsorbed sulfate configurations at the high potentials.

Modes	T(Au–SO_4)	$\delta_s(SO_3)$	$\nu_s(SO_4)$	ν(SO)
Expt.	34	0	−33	59
$SO_4\cdots w_2$*	27	0	−10	34
$SO_4\cdots$w* (w13)	35	20	−17	36
$SO_4\cdots$w* (w12)	34	−5	−13	28
SO_4*	25	−3	−15	30

The configurations containing HSO_4* at the high potentials can be excluded, since their bands at 300–400 and 800–900 cm^{-1} (Figure 3D) cannot match any of those in the measured EC-Raman spectrum. The vibrational modes of the configurations containing HSO_4* have been visualized and listed in Figures S10–S14. Briefly, the EC-Raman spectra reveal that the adstructure must contain the sulfate anions instead of bisulfate anions, but cannot provide strong evidence to determine the number and atomistic arrangements of co-adsorbed water molecules, which might due to the ultraweak cross section of water molecules. Nevertheless, according to joint evidence from the calculated and measured EC-Raman and EC-IR spectra, the Au(111)(√3×√7)-($SO_4\cdots w_2$) configuration is the most plausible adstructure at high potentials.

Adstructure of the Au(111)/H_2SO_4 solution interface at the low potentials. The EC-Raman spectra also show that the band at approximately 300 cm^{-1} gradually appears, and the 614 and 1185 cm^{-1} bands diminish when the potential is negatively shifed to the range of 0.66–0.86 V (low potentials). In addition, the STSs at 243, 956, and 1185 cm^{-1} at high potentials (34, −33, and 59 $cm^{-1}V^{-1}$, respectively) are apparently different from the respective STSs of 24, −25, and 90 $cm^{-1}V^{-1}$ below 0.86 V. The discrepancies of the spectral features at high and low potentials indicate that the interface undergoes a potential-determined structural transformation in the potential range of 0.86–1.06 V.

Although the measured STM image in Figure S15 shows that the interfacial structures at the low potentials may be disordered in the acquisition time domain, the theoretical study based on the Au(111)(√3×√7)-X configurations at low potentials is still relevant to determine approximate adstructures containing sulfate or bisulfate by comparing the calculated EC-Raman spectra with the measured one, as shown in Figure S16 and Table S2–S4. The four configurations containing SO_4* can be excluded at the low potentials, because none of their EC-Raman spectra can interpret the appearance of new band at 300 cm^{-1} and the disappearance of the 1185 cm^{-1} band of the measured EC-Raman spectrum (dark red curves of Figure S16). In contrast, the calculated EC-Raman spectra of $H_sSO_4\cdots$w* (w13) and $H_tSO_4\cdots$w*(w13) to some extend match the measured one. The new Raman band at 300 cm^{-1} is assigned to the $H_2O\cdots HSO_4$ stretching mode ν(HB) (see the modes in Figure S10 and S11). By further comparing the calculated and measured STSs of the three bands in 231–233, 294–301, 966–988 cm^{-1}, as shown in Table S4, we deduce that the adstructure is more likely $H_sSO_4\cdots$w* (w13) than $H_tSO_4\cdots$w* (w13) at low potentials.

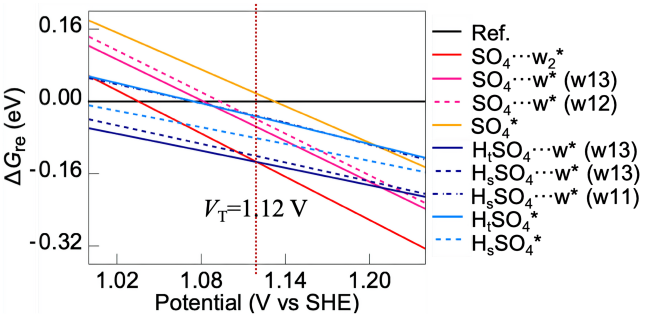

Figure 4. Potential-dependent reaction free energy diagram from 1.00 V to 1.24 V *vs*. SHE. The black line denotes the reference state (HSO_4^-(aq) + $2H_2O$ (aq) + *). The solid and dashed parabolas denote X = H_tSO_4* and H_sSO_4* in blue, $SO_4\cdots$w* (w13) and (w12) in pink, $H_tSO_4\cdots$w* (w13) and $H_sSO_4\cdots$w* (w13) in dark blue.

Reaction free energy diagram and adstructural stability of Au(111)(√3×√7)-X. The potential-dependent reaction free energies ΔG_{re} was calculated to further determine the adstructures at high potentials and the potential-dependent structural transformation. Figure 4 shows that the Au(111)(√3×√7)-($SO_4\cdots w_2$) (solid red line) is the most stable configuration at high potentials. It also shows that $H_tSO_4\cdots$w* (w13) (solid dark blue line) is the most stable structure at low potentials. However, the $H_sSO_4\cdots$w* (w13) (dashed dark blue line) is only slightly less stable than $H_tSO_4\cdots$w* (w13). The ΔG_{re} parabolas of both stable adstructures intersect at 1.12 V *vs*. SHE, which indicates that a deprotonation reaction (Equation 1) occurs when the potential is positively tuned to approximately 1.12 V. In addition, the potential of the deprotonation reaction can slightly depend on the ionic strength I (see Figure S17).

$$HSO_4\cdots w^* + H_2O(aq) - e^- \rightarrow SO_4\cdots w_2{}^* + H^+(aq) \quad (1)$$

To understand the mechanism of the deprotonation reaction, we made a detailed analysis on ΔG_{re}. Figure S18A shows that the adsorbed bisulfate configurations are more stable than the adsorbed sulfate configurations at low potentials, due to the proton affinity of the adsorbed sulfate anion. When the potential is positively shifted, the electrostatic potential energies of the adsorbed sulfate configurations gradually surpass the sum of the proton affinity and the electrostatic potential energies of the adsorbed bisulfate configurations, which stabilizes the sulfate anion adsorption. Moreover, the co-adsorbed water molecules can hydrogen-bond to the O atoms from the adjacent water molecule and O atoms from sulfate anions to effectively stabilize the adstructures, especially at high potentials (Figure S18B).

A limitation of this deprotonation mechanism is that it is obtained on the basis of the ordered Au(111)(√3×√7)-X configurations, a small unit cells compared to the EC-STM images at low potentials (see Fig. S15) that suggest disordered unit cells. Configurations with much larger unit cells such as Au(111)(2√3×5) or (2√3×6) unit cells would be helpful for studying more configurations with lower coverages at low potentials, and obtaining a more complete deportation mechanism of the HSO_4* species.

CONCLUSION

By combining experimental and computational EC-STM, EC-IR, and EC-Raman spectroscopy, we conclude that the adstructure is Au(111)(√3×√7)-(SO_4···w_2) at high potentials (>1.06 V vs SHE); the electro-adsorbed species SO_4···w_2* evolves to H_tSO_4···w* when the potential is negatively tuned. The coadsorbed water molecules play an important role in the structural transformation, which can be further supported by the ΔG_{re} diagram of Au(111)(√3×√7)-X configurations. We found that the potential-dependent interplay between the proton affinity of sulfate anions and the electrostatic potential energy determine the potential-tuned structural transformation on the electrode surface.

This work offers a definite answer that clarifies the 40-year ambiguity in the atomistic adstructure at the Au(111)/H_2SO_4 solution interface at high potentials. The determined adstructure Au(111)(√3×√7)-(SO_4···w_2) straightforwardly enlightens the studies of similar systems, i.e., other M(111)/H_2SO_4 solution interfaces (M = Pt, Rh, Cu, Ir, and Pd). The experimental and computational EC-STM, EC-IR and EC-Raman spectroscopies, and the computational diagram of the reaction free energy may provide a standard workflow to obtain multi-perspective evidence for atomistic structures of the inner Helmholtz plane. The methods thus pave the way to explore the reaction mechanisms of electrocatalytic or photoelectrocatalytic reactions, electro-corrosion and electro-deposition reactions at atomistic levels, and guide the rational design of novel interfacial materials with improved functions and performances.

ASSOCIATED CONTENT

Supporting Information.
Computational details, the calculation of reaction free energy, Figure S1–S19, and Table S1–S4
The Supporting Information is available free of charge on the ACS Publications website.

AUTHOR INFORMATION

Corresponding Author

syding@xmu.edu.cn
bwmao@xmu.edu.cn
juan.feliu@ua.es

Notes

The authors declare no competing financial interest.

ACKNOWLEDGMENTS

The authors acknowledge funding supported by the National Natural Science Foundation of China (91950121, 21727807, 21403179, 21872115, and 21533006). The first-principles calculations in this work were performed on the supercomputing system in the big data system and computing platform of the State Key Laboratory of Physical Chemistry of Solid Surfaces, Xiamen University. Y.F. and S.Y.D. sincerely thank Dr. Ryosuke Jinnouchi for discussion on the calculation of reaction free energy of Au(111)(√3×√7)-X configurations.

REFERENCES

(1) Zaera, F. Probing liquid/solid interfaces at the molecular level. *Chem Rev* **2012,** *112*, 2920-2986.

(2) Schmickler, W.; Santos, E. *Interfacial Electrochemistry*. Oxford University Press: New York, 1996.

(3) Wieckowski, A. *Interfacial Electrochemistry. Theory, Experiment, and Application*. Marcel Dekker: New York, 1999.

(4) White, J. H.; Abruna, H. D. Electrosorption of iodide on platinum(111) studied in situ by X-ray absorption spectroscopy. *J. Phys. Chem.* **1988,** *92*, 7131-7134.

(5) Braunschweig, B.; Mukherjee, P.; Dlott, D. D.; Wieckowski, A. Real-time investigations of Pt(111) surface transformations in sulfuric acid solutions. *J. Am. Chem. Soc.* **2010,** *132*, 14036-14038.

(6) Bodappa, N.; Su, M.; Zhao, Y.; Le, J. B.; Yang, W. M.; Radjenovic, P.; Dong, J. C.; Cheng, J.; Tian, Z. Q.; Li, J. F. Early Stages of Electrochemical Oxidation of Cu(111) and Polycrystalline Cu Surfaces Revealed by in Situ Raman Spectroscopy. *J. Am. Chem. Soc.* **2019,** *141*, 12192-12196.

(7) Kolb, D. M. Electrochemical surface science. *Angew. Chem. Int. Ed.* **2001,** *40*, 1162-1181.

(8) Magnussen, O. M. Ordered Anion Adlayers on Metal Electrode Surfaces. *Chem. Rev.* **2002,** *102*, 679-726.

(9) Scherson, D. A.; Kolb, D. M. Voltammetric curves for Au(111) in acid media: A comparison with Pt(111) surfaces. *J. Electroanal. Chem.* **1984,** *176*, 353-357.

(10) Magnussen, O. M.; Hageböck, J.; Hotlos, J.; Behm, R. J. In situ scanning tunnelling microscopy observations of a disorder-order phase transition in hydrogensulfate adlayers on Au(111). *Faraday Discuss.* **1992,** *94*, 329-338.

(11) Edens, G. J.; Gao, X.; Weaver, M. J. The adsorption of sulfate on gold(111) in acidic aqueous media: adlayer structural inferences from infrared spectroscopy and scanning tunneling microscope. *J. Electroanal. Chem.* **1994,** *375*, 357-366.

(12) Ataka, K.-I.; Osawa, M. In Situ Infrared Study of Water−Sulfate Coadsorption on Gold(111) in Sulfuric Acid. *Langmuir* **1998,** *14*, 951-959.

(13) Shingaya, Y.; Ito, M. Comparison of a bisulfate anion adsorbed on M(111) (M=Pt, Rh, Au, Ag and Cu). *J. Electroanal. Chem.* **1999,** *467*, 299-306.

(14) Nakamura, M.; Shingaya, Y.; Ito, M. Hydration processes on metal surfaces studied by IR and STM: a model for the potential drop across the electric double layers. *Surf. Sci.* **2002,** *502-503*, 474-484.

(15) Cuesta, A.; Kleinert, M.; Kolb, D. M. The adsorption of sulfate and phosphate on Au(111) and Au(100) electrodes: an in situ STM study. *Phys. Chem. Chem. Phys.* **2000,** *2*, 5684-5690.

(16) Shi, Z.; Lipkowski, J.; Gamboa, M.; Zelenay, P.; Wieckowski, A. Investigations of SO42− adsorption at the Au(111) electrode by chronocoulometry and radiochemistry. *J. Electroanal. Chem.* **1994,** *366*, 317-326.

(17) Venkatachalam, S.; Jacob, T. DFT Studies on the Nature of Coadsorbates on SO42-/Au(111). *Z. Phys. Chem.* **2007,** *221*, 1393-1406.

(18) Funtikov, A. M.; Stimming, U.; Vogel, R. Anion adsorption from sulfuric acid solutions on Pt(111) single crystal electrodes. *J. Electroanal. Chem.* **1997,** *428*, 147-153.

(19) Wan, L. J.; Yau, S.-L.; Itaya, K. Atomic Structure of Adsorbed Sulfate on Rh(111) in Sulfuric Acid Solution. *J. Phys. Chem.* **1995,** *99*, 9507-9513.

(20) Li, W.-H.; Nichols, R. J. An in situ STM study of sulphate adsorption on copper(111) in acidic aqueous electrolytes. *J. Electroanal. Chem.* **1998,** *456*, 153-160.

(21) Wan, L.-J.; Hara, M.; Inukai, J.; Itaya, K. In Situ Scanning Tunneling Microscopy of Well-Defined Ir(111) Surface: High-Resolution Imaging of Adsorbed Sulfate. *J. Phys. Chem. B* **1999,** *103*, 6978-6983.

(22) Wan, L.-J.; Suzuki, T.; Sashikata, K.; Okada, J.; Inukai, J.; Itaya, K. In situ scanning tunneling microscopy of adsorbed sulfate on well-defined Pd(111) in sulfuric acid solution. *J. Electroanal. Chem.* **2000,** *484*, 189-193.

(23) Shingaya, Y.; Ito, M. Model double layer structures on M(111) (M=Pt, Rh, Au, Cu and Ag) in a sulfuric acid solution. *Electrochim. Acta* **1998,** *44*, 745-751.

(24) Kolics, A.; Wieckowski, A. Adsorption of Bisulfate and Sulfate Anions on a Pt(111). *J. Phys. Chem. B* **2001,** *105*, 2588-2595.

(25) Jinnouchi, R.; Hatanaka, T.; Morimoto, Y.; Osawa, M. First principles study of sulfuric acid anion adsorption on a Pt (111) electrode. *Phys. Chem. Chem. Phys.* **2012,** *14*, 3208-3218.

(26) Tian, Z.-Q.; Ren, B.; Wu, D.-Y. Surface-Enhanced Raman Scattering: From Noble to Transition Metals and from Rough Surfaces to Ordered Nanostructures. *J. Phys. Chem. B* **2002,** *106*, 9463-9483.

(27) Liu, X.; Wang, D.; Wan, L. Progress of electrode/electrolyte interfacial investigation of Li-ion batteries via in situ scanning probe microscopy. *Science Bulletin* **2015,** *60*, 839-849.

(28) Wang, H.; Zhou, Y.-W.; Cai, W.-B. Recent applications of in situ ATR-IR spectroscopy in interfacial electrochemistry. *Current Opinion in Electrochemistry* **2017,** *1*, 73-79.

(29) Koper, M. T. *Fuel Cell Catalysis: A Surface Science Approach*. John Wiley & Sons, Inc.: Hoboken, New Jersey, 2009.

(30) Li, J. F.; Huang, Y. F.; Ding, Y.; Yang, Z. L.; Li, S. B.; Zhou, X. S.; Fan, F. R.; Zhang, W.; Zhou, Z. Y.; Wu, D. Y.; Ren, B.; Wang, Z. L.; Tian, Z. Q. Shell-isolated nanoparticle-enhanced Raman spectroscopy. *Nature* **2010,** *464*, 392-395.

(31) Li, J. F.; Ding, S. Y.; Yang, Z. L.; Bai, M. L.; Anema, J. R.; Wang, X.; Wang, A.; Wu, D. Y.; Ren, B.; Hou, S. M.; Wandlowski, T.; Tian, Z. Q. Extraordinary enhancement of Raman scattering from pyridine on single crystal Au and Pt electrodes by shell-isolated Au nanoparticles. *J. Am. Chem. Soc.* **2011,** *133*, 15922-15925.

(32) Honesty, N. R.; Gewirth, A. A. Shell-isolated nanoparticle enhanced Raman spectroscopy (SHINERS) investigation of benzotriazole film formation on Cu(100), Cu(111), and Cu(poly). *Journal of Raman Spectroscopy* **2012,** *43*, 46-50.

(33) Li, C. Y.; Le, J. B.; Wang, Y. H.; Chen, S.; Yang, Z. L.; Li, J. F.; Cheng, J.; Tian, Z. Q. In situ probing electrified interfacial water structures at atomically flat surfaces. *Nat. Mater.* **2019,** *18*, 697-701.

(34) Fang, Y.; Dong, J.-C.; Ding, S.-Y.; Cheng, J.; Feliu, J. M.; Li, J.-F.; Tian, Z.-Q. Toward a quantitative theoretical method for infrared and Raman spectroscopic studies on single-crystal electrode/liquid interfaces. *Chem. Sci.* **2020,** *11*, 1425-1430.

(35) Clavilier, J.; Faure, R.; Guinet, G.; Durand, R. Preparation of monocrystalline Pt microelectrodes and electrochemical study of the plane surfaces cut in the direction of the {111} and {110} planes. *J. Electroanal. Chem.* **1980,** *107*, 205-209.

(36) Kresse, G.; Furthmuller, J. Efficient iterative schemes for ab initio total-energy calculations using a plane-wave basis set. *Phys. Rev. B* **1996,** *54*, 11169-11186.

(37) Kresse, G.; Joubert, D. From ultrasoft pseudopotentials to the projector augmented-wave method. *Phys. Rev. B* **1999,** *59*, 1758-1775.

(38) Hammer, B.; Hansen, L. B.; Nørskov, J. K. Improved adsorption energetics within density-functional theory using revised Perdew-Burke-Ernzerhof functionals. *Phys. Rev. B* **1999,** *59*, 7413-7421.

(39) Tersoff, J.; Hamann, D. R. Theory of the scanning tunneling microscope. *Phys. Rev. B* **1985,** *31*, 805-813.

(40) Mathew, K.; Kolluru, V. S. C.; Mula, S.; Steinmann, S. N.; Hennig, R. G. Implicit self-consistent electrolyte model in plane-wave density-functional theory. *J. Chem. Phys.* **2019,** *151*, 234101.

(41) Sato, K.; Yoshimoto, S.; Inukai, J.; Itaya, K. Effect of sulfuric acid concentration on the structure of sulfate adlayer on Au(111) electrode. *Electrochem. Commun.* **2006,** *8*, 725-730.

(42) Suto, K.; Magnussen, O. M. In situ Video-STM studies of sulfate dynamics on Au(111). *J. Electroanal. Chem.* **2010,** *649*, 136-141.

(43) Garcia-Araez, N.; Rodriguez, P.; Navarro, V.; Bakker, H. J.; Koper, M. T. M. Structural Effects on Water Adsorption on Gold Electrodes. *J. Phys. Chem. C* **2011,** *115*, 21249-21257.

(44) Simeone, F. C.; Kolb, D. M.; Venkatachalam, S.; Jacob, T. The Au(111)/electrolyte interface: a tunnel-spectroscopic and DFT investigation. *Angew. Chem. Int. Ed.* **2007,** *46*, 8903-8906.

(45) Ataka, K.-I.; Yotsuyanagi, T.; Osawa, M. Potential-Dependent Reorientation of Water Molecules at an Electrode/Electrolyte Interface Studied by Surface-Enhanced Infrared Absorption Spectroscopy. *J. Phys. Chem.* **1996,** *100*, 10664-10672.

For Table of Contents Only

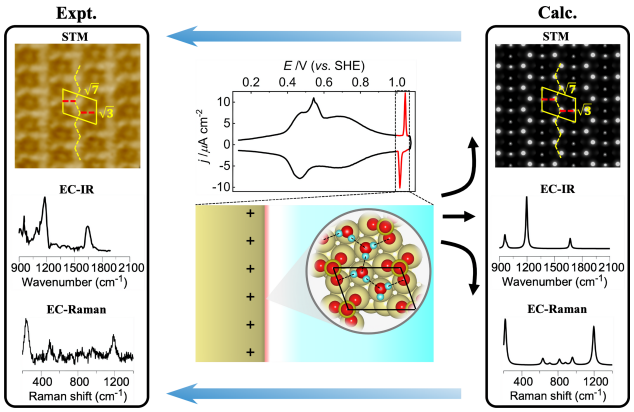

The adstructure with the (√3×√7) symmetry at the interface of Au(111) electrode-sulfuric acid solution was revealed by combining high-resolution electrochemical scanning tuning microscopy, electrochemical Raman spectroscopy, and especially, the newly-developed computational method on electrochemical infrared and Raman spectroscopies.